Dynamical Casimir actuation under non-equilibrium conditions

Tajik, F.; Sedighi, M.; Palasantzas, G.

Published in:
Physics Letters, Section A: General, Atomic and Solid State Physics

DOI:
10.1016/j.physleta.2022.128220

Publication date:
2022

Physics Letters A 443 (2022) 128220

Contents lists available at ScienceDirect

Physics Letters A

www.elsevier.com/locate/pla

Dynamical Casimir actuation under non-equilibrium conditions: The influence of optical properties from different interacting bodies

F. Tajik [a,b], M. Sedighi [c], G. Palasantzas [b,*]

[a] Department of Physics, Faculty of Physics and Chemistry, Alzahra University, Tehran 1993891167, Iran
[b] Zernike Institute for Advanced Materials, University of Groningen, Nijenborgh 4, 9747 AG Groningen, the Netherlands
[c] Institute of Engineering, Hanze University of Applied Sciences, Institute of Engineering, Industrieweg 1, 9402 NP Assen, the Netherlands

ARTICLE INFO

Article history:
Received 9 March 2022
Received in revised form 16 May 2022
Accepted 17 May 2022
Available online 23 May 2022
Communicated by L.M. Woods

Keywords:
Non-equilibrium Casimir force
Chaotic motion
Stable operation
Optical properties

ABSTRACT

In this work we investigated the dynamical actuation of microsystems with non-identical material components in the presence of non-equilibrium Casimir forces between Au and highly doped SiC that show significant difference in conductivity. For autonomous systems, the bifurcation and phase space analysis revealed that when the less conductive material operates at higher temperature, then at short separations the non-equilibrium force causes instability. Furthermore, for periodically driven systems the Melnikov function and Poincare portrait analysis showed that the devices are more robust against chaotic motion when the less conductive component is at low temperature at short separations. At larger separations chaotic behavior is more likely to occur for systems with the more conductive component at higher temperature.

1. Introduction

Dispersion forces are genuine in nature and originate form quantum fluctuations of the electromagnetic field between uncharged bodies in vacuum and/or in a material medium. These forces cover both the van der Waals (short-range) and Casimir (long-range) asymptotic regimes [1–5]. By the advancement in micro/nanofabrication and consequent reduction of the scale of microdevices into the submicron range, the role of Casimir and electrostatic forces could become comparable [6–9]. Due to large surface areas and separation gaps small enough, it is feasible the Casimir force to play a remarkable role and under certain conditions to drag mechanical elements together leading to permanent adhesion and device malfunction [6–9]. Hence, by miniaturizing the micro electromechanical systems (MEMS) technology towards nano electromechanical systems (NEMS), the correct estimation of the magnitude of the Casimir force as an omnipresent force between components is essential for the design of micro/nano systems [6–9].

The Casimir force was proposed in 1948 by the Dutch physicist Hendrik Casimir [10], who recognized that the force is due to perturbation of the zero-point energy by assuming two perfectly reflecting parallel plates. Soon after, Lifshitz and co-workers in the 1950s [11] presented a general macroscopic theory, which elaborates the forces via the dielectric response of the interacting bodies and the intervening medium relating the dissipative properties of the plates (due to optical absorption by many microscopic dipoles) and the resulting electromagnetic (EM) fluctuations. This theory covers both the Casimir (long-range) and van der Waals (short-range) regimes [11–14]. Furthermore, the dependence of the Casimir force on material optical properties provides the opportunity to tailor the force using the appropriate choice of the interacting materials [15–24]. Besides the optical properties, extensive investigations have been done to reveal the effect of corrugation of surface [25–27], thermal effect [28–30] and surface roughness [31] on the magnitude of the Casimir force. So far, some studies have shown the strong dependency of the material optical properties on the thermal effect, which consequently defines the magnitude of both the thermal equilibrium and non-equilibrium Casimir forces.

Although the role of the thermal effect on the dynamic stability of devices consisting of identical materials has been explored [32,33], it remains unexplored how the device performance consisting of non-identical bodies can be affected by thermal fluctuation under non-

* Corresponding author.
E-mail address: g.palasantzas@rug.nl (G. Palasantzas).

https://doi.org/10.1016/j.physleta.2022.128220

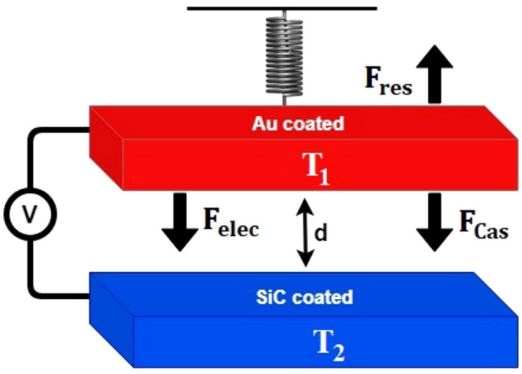

Fig. 1. Schematic of the microdevice under consideration, where the acting forces on the moving plate are illustrated.

equilibrium conditions. This leads us to investigate the non-equilibrium Casimir force in MEMS with significant difference in the optical properties between its interacting components. Hence, we will address how the low and high conductive components can influence the non-equilibrium Casimir force and consequently the actuation dynamics of microdevices by changing their temperature and taking precisely into account the optical properties at low frequencies. For the latter the measurement of the optical data is not feasible and extrapolation in necessary [33–35]. Moreover, in order to have a realistic view for the study and design of MEMS, it is crucial to take into account the chaotic motion as an unavoidable problem that can lead to device malfunction. Therefore, we have studied the conditions that can enhance the occurrence of chaotic behavior in devices, which could lead to irreversible adhesion between components during long-term operation. Eventually, this study can provide substantial knowledge for the modeling a microsystem that operate under non-equilibrium conditions, and add the novel possibility to device design by considering the precise modeling of the material optical properties.

2. Optical properties of materials and modeling of dynamical systems

In order to cover a wide range of materials with diverse optical properties, we have chosen Au as a good metal conductor [4,5,20], and nitrogen doped SiC as a poor conductor though it is a material suitable for operation in harsh environments [36,37]. In the Drude model, using the plasma frequency ω_p and the damping factor ω_τ, which are obtained from the analysis of the optical data (see Fig. A1, Supplemental Material), the static conductivity of the materials $\sigma = (\omega_p^2/\omega_\tau)/4\pi$ can be estimated. For SiC we obtained $\omega_p^2/\omega_\tau = 0.4$ eV [36], and for Au $\omega_p^2/\omega_\tau = 1600$ eV [20,21]. These values demonstrate a conductivity contrast for Au/SiC more than three orders of magnitude. Subsequently, from the measured optical properties we calculated the corresponding dielectric functions at imaginary frequencies $\varepsilon(i\xi)$ as in (see Supplemental Material Appendix A) [32,33], which are essential for the calculation of the Casimir force via Lifshitz theory (see Supplemental Material Appendix B).

Furthermore, in order to analyze the effect of the non-equilibrium Casimir force on the dynamics performance, it is assumed a simplified MEMS composed from two electrodes operating at different temperature [1–5]. The fixed electrode is assumed to be coated with SiC, and the moving one is with Au (see Fig. 1). The latter is supported from a mechanical spring that can be described by the Hooke's law. The elastic restoring force $F_{res} = K(d - z)$ that originates from the spring with stiffness K, operates against the attractive Casimir force. The non-equilibrium Casimir force between two non-identical components at temperatures T_1 and T_2 is denoted as $F_{Cas}(T_1, T_2, z) = F_0(z) + F_{th}^{neq}(T_1, T_2, z)$. Here the first term describes the zero temperature contribution whereas the second part, which consists of propagating $F_{th}^{neq,\ PW}(T, z)$ and evanescent waves $F_{th}^{neq,\ EW}(T, z)$, describes the thermal fluctuations (see Supplemental Material Appendix A). It is necessary to mention that we are considering significantly thick electrodes (than the mean free path of charge carriers), and the components of the Casimir force are obtained using the Lifshitz theory between two half spaces. Moreover, in this study the dielectric function is independent on temperature and all the data have been measured at room temperature. Thus, in order to present more accurate data analysis, it is necessary to consider the influence of the temperature in $\varepsilon(\omega)$ [38]. Eventually, the equation of motion for the actuating system (see Fig. 1) is given by

$$M\frac{d^2z}{dt^2} + \left(\frac{M\omega_0}{Q}\right)\frac{dz}{dt} = -F_{res} + F_{Cas} + \gamma F_0^{ext}\cos(\omega t)\,. \tag{1}$$

In Eq. (1) M is the mass of the moving plate, and the term $(M\omega_0/Q)(dz/dt)$ defines the intrinsic energy dissipation of the system. The conservative system is supposed to be a MEMS with a high quality factor $Q > 10^4$ [39] so that energy dissipation effects is negligible. The frequency ω_0 is considered similar to the dynamic mode atomic force microscope cantilevers or other MEMS (typically $\omega = 300\ kHz$) [39]. The parameter γ describes the difference between the conservative autonomous operating system ($\gamma = 0$), and the non-conservative driven system by an applied periodic force and dissipation effects using a finite quality factor Q ($\gamma = 1$). In addition, we considered surfaces without roughness. This is because by scaling down into nanometers the roughness yields remarkable contribution at separations smaller than 100 nm, while in our analysis we considered larger initial separations between the components in the ranges 200 nm $< d <$ 4500 nm. Moreover, the lateral dimensions of the interacting plates are assumed to be $L_x = L_y = 10$ μm.

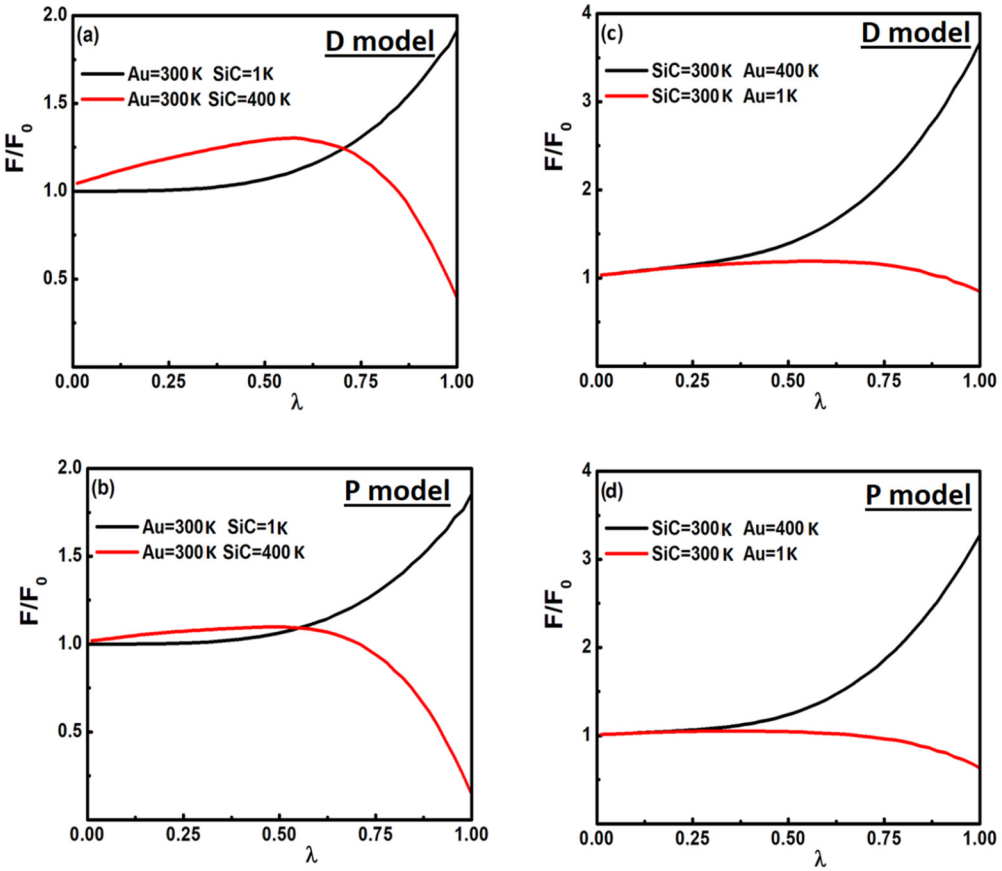

Fig. 2. Plots of the force ratio F $(= F_0 + F_{th}^{neq})/F_0$ vs. λ (z/d with d = 4500 nm) under non-equilibrium conditions for the Au- SiC interacting systems. The temperature of the components and the method of extrapolation at low frequencies are indicated.

3. Results and discussion

3.1. Out of thermal equilibrium Casimir force between Au-SiC systems

The first part of this study is devoted to calculations of the Casimir force between non-identical interacting components at different temperatures. The results clearly illustrate that by interchanging the temperature of the non-identical components can induce a strong change in the non-equilibrium force [28]. Here, we considered a large temperature difference between the interacting components in order to show more clearly how the optical properties can influence the contribution of the non-equilibrium thermal force. Fig. 2, which displays the relative values between total force $(F_0 + F_{th}^{neq})$ with respect to the part that corresponds to zero point fluctuation (F_0) versus surface separation, shows that the Casimir force is stronger at higher temperature and short separations when a less conductive component is present. However, at large separations the opposite takes place and the temperature of the more conductive component plays key role on the magnitude of the Casimir force. It should be clarified that the evanescent components $(F_{th}^{neq,\ EW})$ yields the major contribution to the force at short separations, while it decays quickly by increasing the separation and at larger separations the propagating component $(F_{th}^{neq,\ PW})$ plays crucial role. The calculations indicate that the evanescent components reveal significant dependence on the SiC component at higher temperature, while the propagating part reveals more sensitivity to the Au component. This part is significant and preserves its strength over wider separations, when Au is placed at higher temperature. And it is also negative at large separations if the temperature of SiC becomes higher than that of Au. As a result $F/F_0 < 1$ at large separations when the hot component is SiC.

In any case, the differences between the Au-Au and the Au-SiC systems (see also Fig. A2, Supplemental Material Appendix B) are significant, and possibly can be measured at separations above 200 nm taking into account the successful force measurements at larger separations for Au-Au interacting bodies [3–5,40]. Finally, the sensitivity of the force to the Drude and Plasma models (see Supplemental Material Appendix A) is significantly stronger in MEMS where the non-equilibrium thermal condition varies by changing the temperature of its poorly conducting component. As Figs. 2a and 2b indicate, the influence of the thermal correction becomes weaker by for the Plasma model. This is because there is no extrapolation of the dielectric function at rear low frequencies, which eventually lead to reduction of the differences in these ranges.

3.2. Conservative systems ($\gamma = 0$)

For the conservative system it is convenient to introduce the bifurcation parameter $\delta_{Cas} = F_{Cas}^{m}/kd$ [41–43] which is the ratio of the minimum of Casimir force to the maximum restoring force. The parameter δ_{Cas} determines when there is a closed orbit solution for the motion of the microdevice indicating the existence of sufficient restoring force to prevent the occurrence of permanent adhesion [42]. Using δ_{Cas}, Eq. (1) can be rewritten in this form (for $\gamma = 0$)

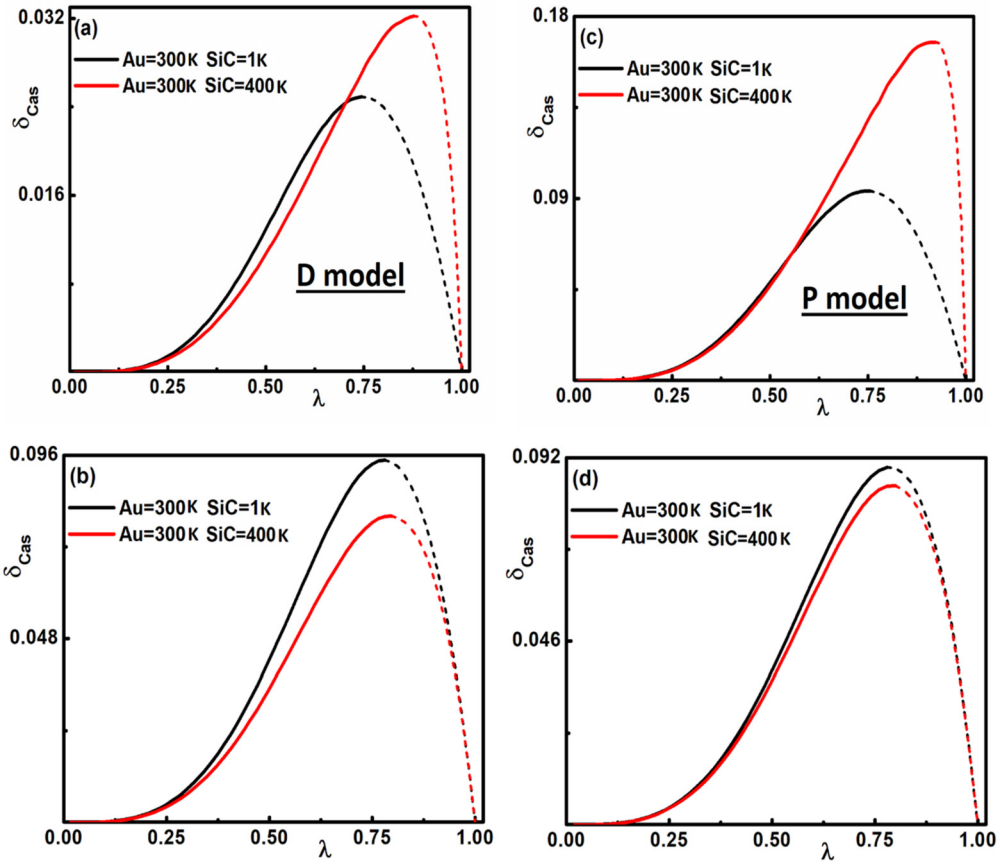

Fig. 3. Bifurcation diagrams δ_{Cas} vs λ $(=z/d)$ for the Au-SiC system under non-equilibrium conditions, where the Au component is fixed at 300 K and the temperature of SiC is indicated. For the left column (a and b) the Drude model is used, and for the right column (c and d) the Plasma model. In the upper row (a and c) the initial distance (d) is 4200 nm, and for lower row (b and d) it is 1900 nm. The solid and dashed lines represent the unstable and stable equilibrium points, respectively.

$$\frac{d^2\lambda}{dT^2}+\left(\frac{1}{Q}\right)\frac{d\lambda}{dT}=-(1-\lambda)+\delta_{Cas}\frac{F_{Cas}}{F_{Cas}^{m}}+\varepsilon\frac{F_0^{ext}}{F_{res}^{Max}}\cos\left(\frac{\omega}{\omega_0}T\right) \tag{2}$$

with $\lambda=z/d$ and $T=\omega_0 t$. The bifurcation diagrams in Figs. 3 and 4 display how the effect of the thermal corrections on the unstable and stable regions depends on the temperature and the conductivity of the interacting components. The two equilibria points appear when the restoring force becomes sufficiently strong so that $\delta_{Cas}<\delta_{Cas}^{Max}$. The stationary points closest to the initial separation ($\lambda=1$) are stable centers with closed orbit or equivalently periodic solutions around them. Furthermore, the so-called unstable points are located near to the fixed plate, and the motion around them will lead to irreversible adhesion on the fixed electrode due to the Casimir force. These plots indicate that the thermal contribution makes remarkable changes on the actuation of MEMS. This is also reflected in Fig. 5 that shows how λ_c (corresponding to $\delta_{Cas}{}^{Max}$) changes for different temperatures of the less conductive (SiC) component.

In Fig. 3a and 3b, using the Drude model, the more conductive component is fixed at 300 K and the temperature of the less conductive part varies from low to high temperatures. It is obvious by considering the initial short separation (Fig. 3b), then an increasing temperature of Au leads to enlargement of the stable performance, while these changes become weaker in Fig. 3d depending on the model used for the extrapolation. In the case of a large initial separation (Figs. 3a and 3c), the opposite takes place for both the Plasma and Drude models. Moreover, Fig. 4 shows that the dependence on the method of extrapolation disappears when the less conductive component is fixed at 300K, and the temperature of the more conductive varies from low to high temperatures. Indeed, the system with colder the SiC component reveals weaker stability and there is no sensitivity to the model of extrapolation.

In addition to the bifurcation analysis, the sensitive dependence of the actuation dynamics on the thermal effect can be captured by the Poincare maps shown in Figs. 6 to 8. The homoclinic orbit establishes the separation between unstable motion, which leads to stiction within one period for the autonomous microdevice, from the closed periodic orbits around the stable point. According to Figs. 6 and 7, by increasing the temperature of the less conductive component the stability of the device increases for large distance between the components in both the Plasma and Drude models. The opposite takes place for short separations. Fig. 8 shows also that by decreasing the temperature of the more conductive component leads to enlargement of the homoclinic orbit or equivalently the stable area of operation over a wider region. Therefore, the non-equilibrium thermal corrections to the Casimir force have remarkable impact on conservative actuation depending also on the optical properties of the interacting materials.

3.3. Non-conservative systems ($\gamma=1$)

Furthermore, it is investigated the chaotic behavior of the actuating device by an external periodic force $F_0^{ext}\cos(\omega t)$ [44]. Here it is supposed that the motion occurs in clean and dry conditions. Moreover, capillary and hydrodynamic forces, which can be significant under ambient conditions, are not considered here. After rescaling all terms to F_0^{ext}, the term related to the driving force is small compared to

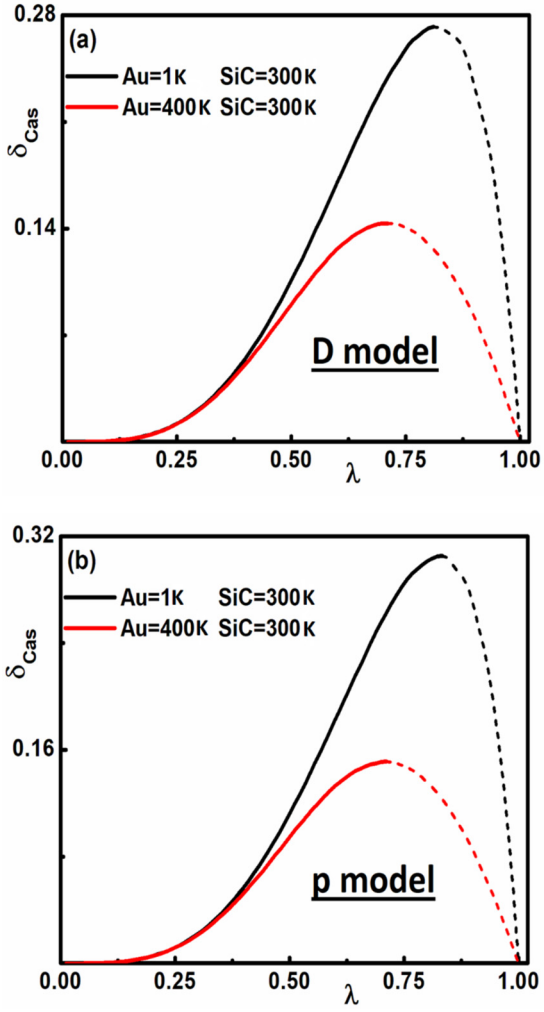

Fig. 4. Bifurcation diagrams δ_{Cas} vs λ $(=z/d)$ for the Au- SiC system under non-equilibrium conditions. The SiC component is fixed at 300 K and the temperature of Au, as well as the method of extrapolation are indicated. The initial distance (d) is 3500 nm.

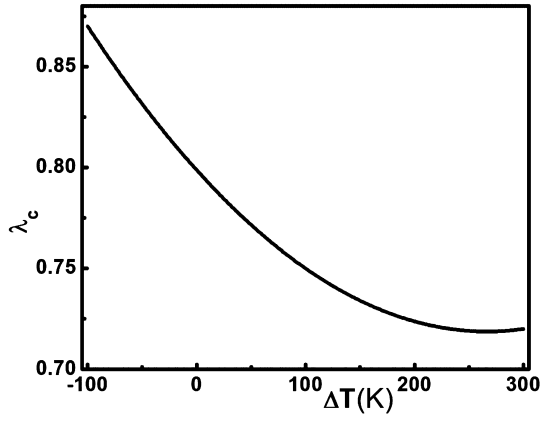

Fig. 5. Diagrams of λ_c (corresponding to $\delta_{cas}{}^{Max}$) vs. ΔT $(=T_{Au}\text{-}T_{SiC})$. The Au component is fixed at 300 K, and the temperature of SiC changes from 400 K to 1 K. Here we considered the initial distance d=4200 nm.

the other forces (since $|\cos(\omega t)| < 1$). Thus, the source of the chaotic motion will be the splitting of the separatrix of the conservative system, which by the Smale-Birkhoff homoclinic theorem [45] yields the occurrence of chaotic motion. In the first-order approximation of the non-conservative system, the so called Melnikov function can provide a solution to the splitting of separatrix [45,46]. As a first-order perturbation on a conservative system, the so called Melnikov function can be introduced:

$$M(T_0) = \int_{-\infty}^{+\infty} \frac{d\varphi_{hom}^{C}(T)}{dT}\left[-\frac{\sigma\omega_0 d}{F_0^{ext}}\frac{d\varphi_{hom}^{C}(T)}{dT} + \cos\left[\omega(T+T_0)\right]\right]dT. \tag{3}$$

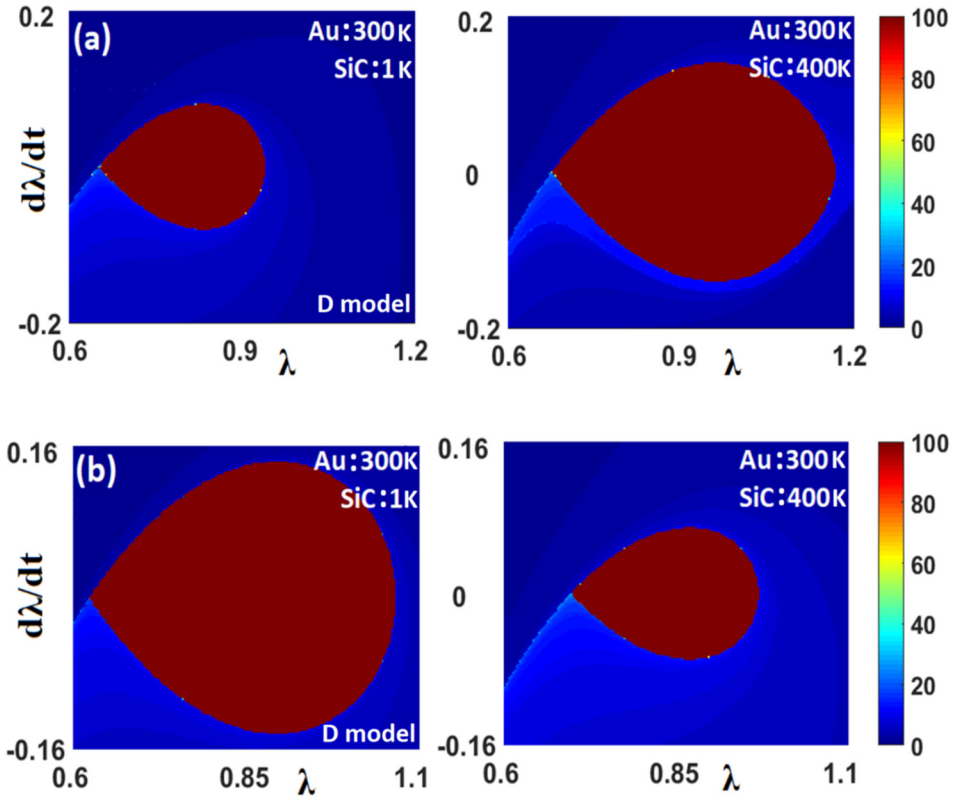

Fig. 6. Contour phase space plots $d\lambda/dt$ vs. λ for the Au-SiC system under non-equilibrium conditions, where the Au component is fixed at 300K, and the temperature of SiC as well as the method of extrapolation are indicated. For the computation it is used 200×200 initial conditions $(\lambda, d\lambda/dt)$. The elliptical in shape homoclinic orbit encloses the initial conditions that lead to stable oscillations. In (a) $\delta_{Cas} = 0.02$ and d=4500 nm, and in (b) $\delta_{Cas} = 0.073$ and d=1900 nm.

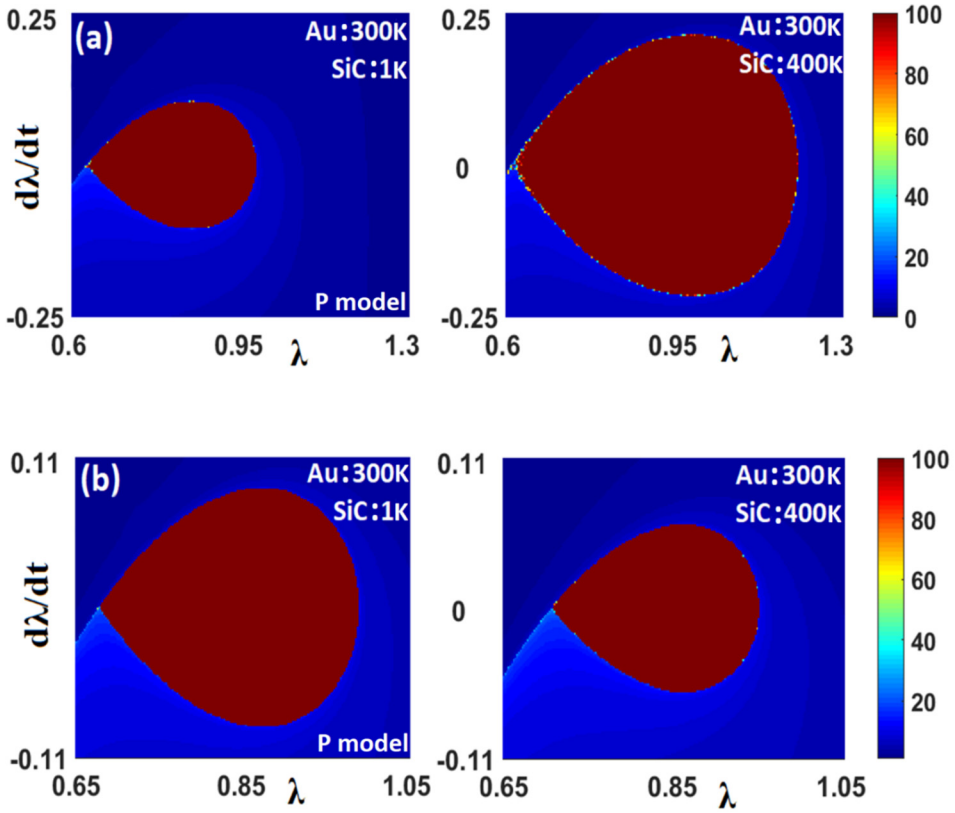

Fig. 7. Contour phase space plots $d\lambda/dt$ vs. λ for the Au-SiC system under non-equilibrium conditions where the Au component is fixed at 300 K and the temperature of SiC as well as the method of extrapolation are indicated. For the calculations we used 200×200 initial conditions $(\lambda, d\lambda/dt)$. The elliptical in shape homoclinic orbit encloses the initial conditions that lead to stable oscillations. In (a) $\delta_{Cas} = 0.08$ and d=4200 nm, and in (b) $\delta_{Cas} = 0.08$ and d=1900 nm.

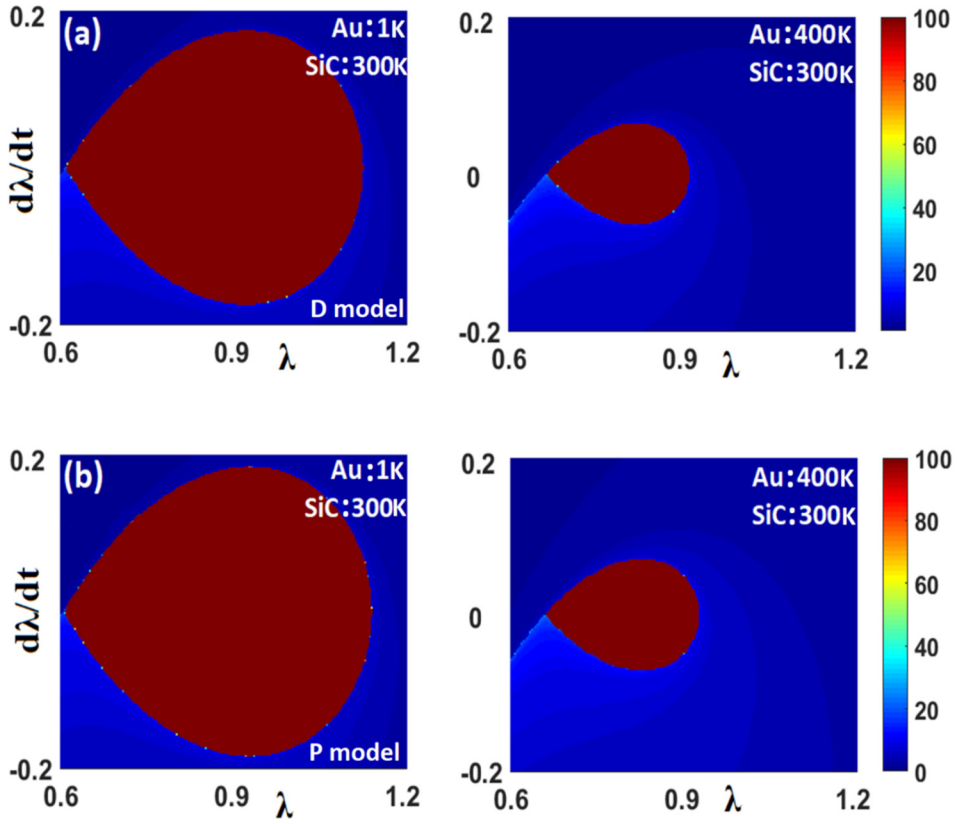

Fig. 8. Contour phase space plots dλ/dt vs. λ for the Au-SiC system under non-equilibrium conditions, where the SiC component is fixed at 300 K and temperature of Au as well as the method of extrapolation are indicated. For the computation we used 200 × 200 initial conditions (λ, dλ/dt). The elliptical in shape homoclinic orbit encloses the initial conditions that lead to stable oscillations. The initial distance is d=3500 nm and $\delta_{Cas} = 0.13$.

The homoclinic solution of the conservative system is denoted as $\varphi^{C}_{hom}(T)$. By considering

$$\int_{-\infty}^{+\infty} (d\varphi^{C}_{hom}(T)/dT)^2 dT = < (d\varphi^{C}_{hom}(T)/dT)^2 > \text{ and } \alpha = \sigma\omega_0 d/F_0^{ext} \ (\sigma = M\omega_o/Q),$$

the Eq. (6) can be written as:

$$M(T_0) = -\alpha < (\frac{d\varphi^{C}_{hom}(T)}{dT})^2 > + A(\omega)\cos[\omega(T_0 + \varphi(\omega))]. \tag{4}$$

The term $A(\omega)\ \cos[\omega(T_0 + \varphi(\omega))]$ is the real part of the Fourier transform of $d\varphi^{C}_{hom}(T)/dT$. Therefore, if we define

$$\mu^{c}_{hom} = < (\frac{d\varphi^{C}_{hom}(T)}{dT})^2 > . \quad \text{and} \quad \beta(\omega) = \left| H\left[Re\left(F\left\{ \frac{d\varphi^{C}_{hom}(T)}{dT} \right\} \right) \right] \right|, \tag{5}$$

where H[...] denotes the Hilbert transform [44,47], then the threshold condition for chaotic motion to take place $\alpha = \beta(\omega)/\mu^{c}_{hom}$ obtains the form

$$\alpha = \frac{\sigma\omega_{0d}}{F_0^{ext}} = \left| H\left[Re\left(F\left\{ \frac{d\varphi^{C}_{hom}(T)}{dT} \right\} \right) \right] \right| / < (\frac{d\varphi^{C}_{hom}(T)}{dT})^2 > \tag{6}$$

Eqs. (3) and (4) are valid only for the case of an additive perturbative force in Eq. (1). And it is possible to replace $F_{Cas}(z)$ with another nonlinear function of z [48].

Figs. 9 and 10 show the threshold curves $\alpha = \sigma\omega_0 d/F_0^{ext}$ vs. driving frequency ratio ω/ω_o. For the area above the curve, where the magnitude of α is significant, the influence of the driving force is negligible as compared to dissipation ($\alpha \sim \sigma/F_0^{ext}$). As a result the motion goes finally towards the stable periodic orbit of the conservative system. While in lower part of curve, where the magnitude of α is weak, the separatrix starts to split leading possibly to chaotic motion. Clearly for the Au-SiC system with large initial operation distance, by placing Au at 300 K and increasing the temperature of SiC from 1 K to 400 K, the thermal fluctuations lead to decrease in the possibility for chaotic motion for both the Plasma and Drude models (Figs. 9a and 9c). Furthermore, by considering small initial separations, according to Figs. 9b and 9d, then by increasing the temperature of SiC the device loses its stability sooner increasing the risk of chaotic motion. In Fig. 10 the temperature of the less conductive part is fixed at 300 K, and the temperature of the more conductive component varies from 1 K to 400 K. In this case, for small separations the change in temperature of the Au plate does not influence the

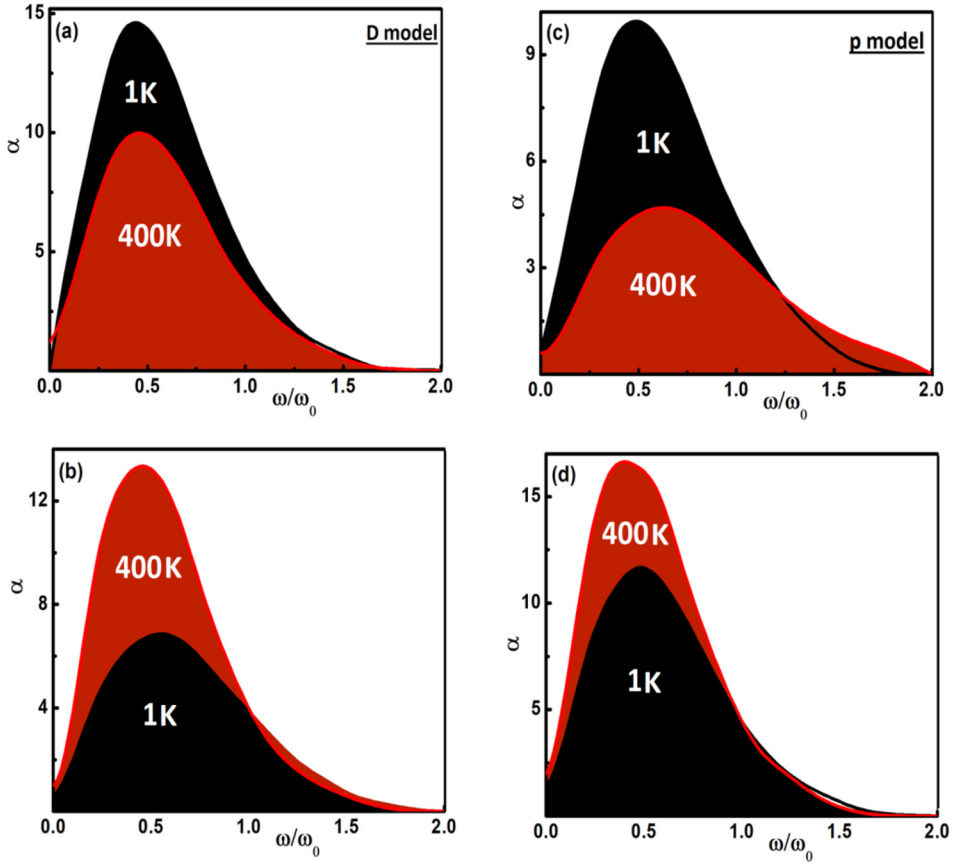

Fig. 9. Threshold curve α $(=\sigma\omega_0 d/F_0^{ext})$ vs. driving frequency ω/ω_o (with ω_o the natural frequency of the system) to compare the influence of thermal effects under non-equilibrium conditions for the Au-SiC system. Au component is fixed at 300 K and temperature of SiC is indicated. For left column (a and b) Drude model and for right column (c and d) Plasma model is used. In the upper row (a and c) the initial distance is d=4200 nm, and for lower row (b and d) d=1900 nm. In (a) $\delta_{Cas} = 0.036$, (b) $\delta_{Cas} = 0.07$, and in (c) and (d) $\delta_{Cas} = 0.08$.

thermal contribution (see also Figs. 2c and 2d) and as a result the possibility of chaotic behavior for both extrapolation models. However, at large separations chaotic motion is more possible to take place in systems with a hot Au plate for both the Plasma and Drude models.

Chaotic motion can be further analyzed using the sensitive dependence of the motion on its initial conditions via the Poincare maps as it is shown in Figs. 11 and 12. When chaotic motion occurs (with decreasing value of α), a region of initial conditions can be seen where the sharp border between distinct solutions is not obvious. For chaotic motion, the absence of a sharp boundary is demonstrated between the blue and the red regions. As a result, if the motion is chaotic then stiction can still takes place between the interacting plates after several oscillation and influence the long-term stable performance of the system [32,33]. Therefore, chaotic behavior introduces significant risk for device malfunction due to stiction, and by increasing the Casimir force our ability to predict the long term performance of the system becomes more limited.

For the Au-SiC system by placing the interacting plates at a large initial separation (Fig. 11a) and set the Au component at 300K, the thermal corrections are more effective to decrease the possibility of chaotic motion and enlarge the stable operation by decreasing the temperature of the SiC plate in both the Plasma and Drude models. However, according to Fig. 11b, for a small initial distance between the components the thermal corrections of the Casimir force, and consequently the stable actuation reveals the reverse order. If we compare the Poincare maps of Fig. 12a and 12b by setting the temperature of the SiC part at 300 K and increase the temperature of the Au plate from 1 K to 400 K, the possibility of chaotic behavior starts to increase and the device loses sooner its stability. In this case the magnitude of the thermal corrections, and as a consequence the stable operation of the device do not show any sensitivity to the method of extrapolation at low frequencies that distinguishes the Plasma and Drude models. It would interesting in the future, however, the present studies about chaotic behavior to be further extended by incorporating also non-local effects on the optical properties [49].

4. Conclusions

In conclusion, we have studied the dynamical actuation of systems with non-identical components in the presence of non-equilibrium Casimir forces. For this purpose, we considered the Casimir interaction between Au and highly doped SiC because of their significant difference in conductivity, as well as the Drude and Plasma models have been applied for extrapolation of the optical properties at low frequencies, where it is not feasible to do measurements. For frictionless autonomous systems, bifurcation and phase space analysis revealed that when the less conductive material is at higher temperature, then at short distances the non-equilibrium Casimir force causes instability. However, at larger distances the reduction of the thermal effect allows for a wider range of stable operation. Moreover, the variation of the non-equilibrium Casimir force and consequently the stable performance of devices that is produced by changing the temperature of the less conductive component, reveals a sensitive dependence on the model to extrapolate the optical data at low frequencies. Finally, for driven system the Melnikov function and Poincare portrait analysis have illustrated that the devices can be more

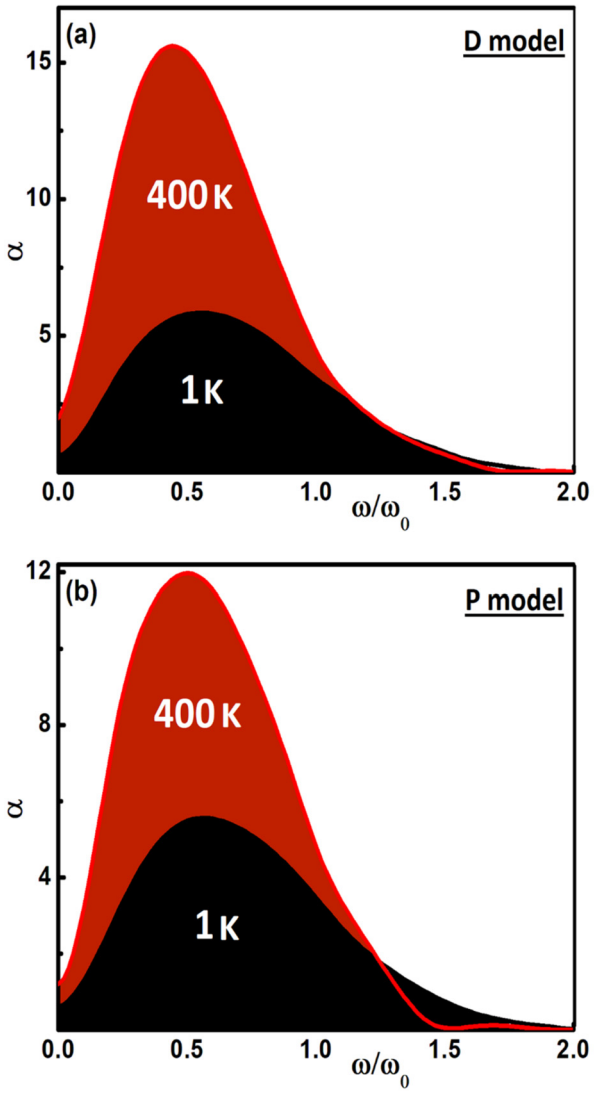

Fig. 10. Threshold curve α $(=\sigma\omega_0 \mathrm{d}/F_0^{ext})$ vs. driving frequency ω/ω_o (with ω_o the natural frequency of the system) to compare the influence of thermal effects under non-equilibrium conditions for the Au-SiC system. The SiC component is fixed at 300 K and the temperature of Au and method of extrapolation is indicated. The initial distance is d=3500 nm and $\delta_{\mathrm{Cas}} = 0.05$.

robust against chaotic motion when the less conductive component is at low temperature and operating at short separations. At large separations chaotic behavior is more likely to occur for systems with the more conductive component at higher temperature. Therefore, non-equilibrium Casimir forces are able to affect the long term dynamics operation of a driven device, but any analysis must take carefully into account their significant dependency on the optical properties and the conductive state of the interacting materials.

CRediT authorship contribution statement

F. Tajik: Methodology, Investigation, Formal analysis, Conceptualization, Writing – original draft. **M. Sedighi:** Conceptualization, Writing – original draft, Writing – review & editing. **G. Palasantzas:** Writing – review & editing, Conceptualization.

Declaration of competing interest

The authors declare the following financial interests/personal relationships which may be considered as potential competing interests: George Palasantzas reports financial support was provided by University of Groningen Zernike Institute for Advanced Materials. Fatemeh Tajik reports financial support was provided by Alzahra University. Mehdi Sedighi reports financial support was provided by Hanze University of Applied Sciences.

Acknowledgements

G. P. acknowledges support from the Zernike Institute for Advanced Materials at University of Groningen. F. T. acknowledges support from the Department of Physics at Alzahra University.

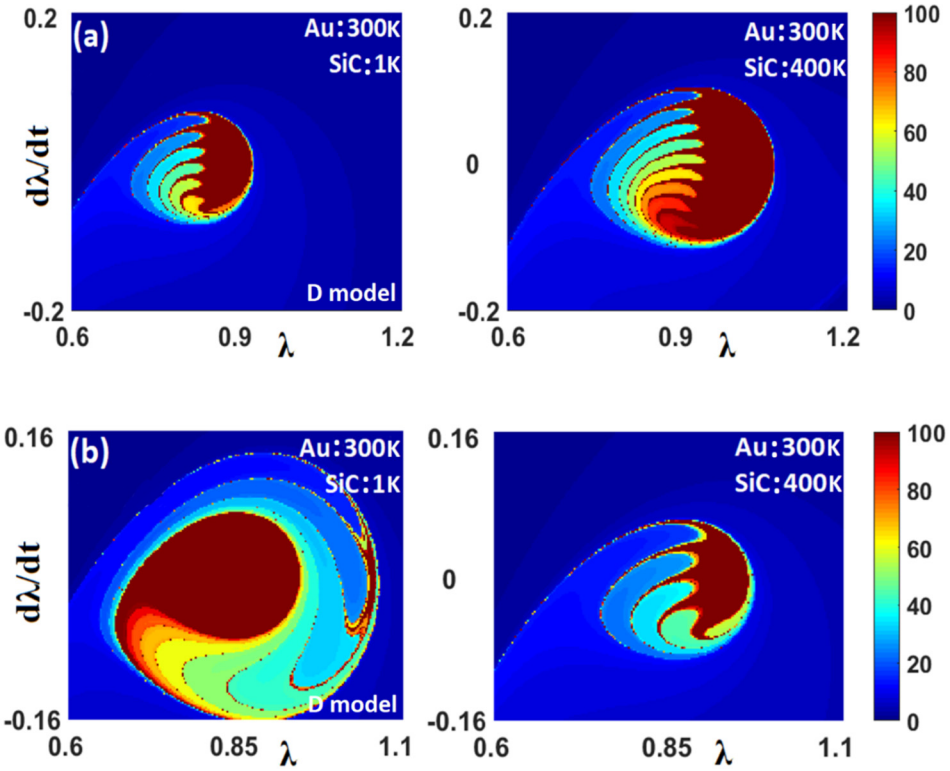

Fig. 11. Contour plot of the transient times to stiction using Poincare phase maps $d\lambda/dt$ vs. λ for the non-conservative Au-SiC system, where the Au component is fixed at 300 K and the temperature of SiC as well as the method of extrapolation are indicated. For the computation we used 200×200 initial conditions $(\lambda, d\lambda/dt)$. We have considered $\alpha = 2$ and $\omega/\omega_0 = 0.5$. In (a) $\delta_{Cas} = 0.02$ and d=4200 nm, and in (b) $\delta_{Cas} = 0.073$ and d=1900 nm. (For interpretation of the colors in the figure(s), the reader is referred to the web version of this article.)

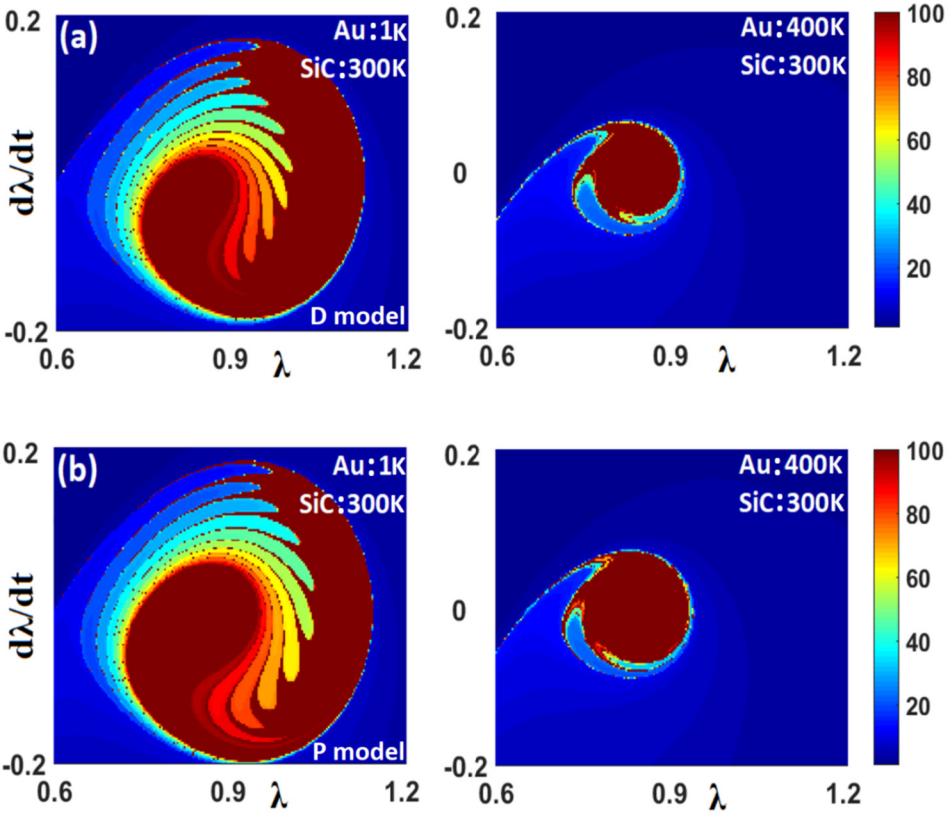

Fig. 12. Contour plot of the transient times to stiction using Poincare phase maps $d\lambda/dt$ vs. λ for the non-conservative Au-SiC system where the SiC component is fixed at 300 K and temperature of Au as well as the method of extrapolation are indicated. For the computation we used 200×200 initial conditions $(\lambda, d\lambda/dt)$. We have considered $\alpha = 1.8$ and $\omega/\omega_0 = 0.7$. The initial distance is d=3500 nm and $\delta_{Cas} = 0.13$.

Appendix A. Supplementary material

Supplementary material related to this article can be found online at https://doi.org/10.1016/j.physleta.2022.128220.

References

[1] A.W. Rodriguez, F. Capasso, S.G. Johnson, Nat. Photonics 5 (2011) 211.
[2] F. Capasso, J.N. Munday, D. Iannuzzi, H.B. Chan, IEEE J. Sel. Top. Quantum Electron. 13 (2007) 400.
[3] M. Bordag, G.L. Klimchitskaya, U. Mohideen, V.M. Mostepanenko, Oxford University Press, New York, 2009.
[4] R.S. Decca, D. L´opez, E. Fischbach, G.L. Klimchitskaya, D.E. Krause, V.M. Mostepanenko, Ann. Phys. (NY) 318 (2005) 37.
[5] R.S. Decca, D. L´opez, E. Fischbach, G.L. Klimchitskaya, D.E. Krause, V.M. Mostepanenko, Phys. Rev. D 75 (2007) 077101.
[6] F.M. Serry, D. Walliserand, G.J. Maclay, J. Appl. Phys. 84 (1998) 2501.
[7] F.M. Serry, D. Walliser, G.J. Maclay, J. Microelectromech. Syst. 4 (1995) 193.
[8] F.W. DelRio, M.P. de Boer, J.A. Knapp, E.D. Reedy Jr., P.J. Clews, M.L. Dunn, Nat. Mater. 4 (2005) 629.
[9] G. Palasantzas, J.T.M. DeHosson, Phys. Rev. B 72 (2005) 121409.
[10] H.B.G. Casimir, Proc. K. Ned. Akad. Wet. 51 (1948) 793.
[11] E.M. Lifshitz, Sov. Phys. JETP 2 (1956) 73.
[12] I.E. Dzyaloshinskii, E.M. Lifshitz, L.P. Pitaevskii, Sov. Phys. Usp. 4 (1961) 153.
[13] P. Ball, Nature 447 (2007) 77.
[14] H.G. Craighead, Science 290 (2000) 1532.
[15] F. Chen, G.L. Klimchitskaya, V.M. Mostepanenko, U. Mohideen, Opt. Express 15 (2007) 4823.
[16] G. Torricelli, I. Pirozhenko, S. Thornton, A. Lambrecht, C. Binns, Europhys. Lett. 93 (2011) 51001.
[17] S. de Man, K. Heeck, R.J. Wijngaarden, D. Iannuzzi, Phys. Rev. Lett. 103 (2009) 040402.
[18] G. Torricelli, P.J. van Zwol, O. Shpak, C. Binns, G. Palasantzas, B.J. Kooi, V.B. Svetovoy, M. Wuttig, Phys. Rev. A 82 (2010) 010101(R).
[19] G. Torricelli, P.J. van Zwol, O. Shpak, G. Palasantzas, V.B. Svetovoy, C. Binns, B.J. Kooi, P. Jost, M. Wuttig, Adv. Funct. Mater. 22 (2012) 3729.
[20] V.B. Svetovoy, P.J. van Zwol, G. Palasantzas, J.Th.M. DeHosson, Phys. Rev. B 77 (2008) 035439.
[21] G. Bimonte, Phys. Rev. A 83 (2011) 042109.
[22] F. Tajik, M. Sedighi, M. Khorrami, A.A. Masoudi, G. Palasantzas, Phys. Rev. E 96 (2017) 042215.
[23] F. Tajik, M. Sedighi, M. Khorrami, A.A. Masoudi, H. Waalkens, G. Palasantzas, Phys. Rev. E 98 (2018) 02210.
[24] F. Tajik, Z. Babamahdi, M. Sedighi, G. Palasantzas, Universe 7 (2021) 123.
[25] M.F. Miri, R. Golestanian, Appl. Phys. Lett. 92 (2008) 113103.
[26] A. Ashourvan, M.F. Miri, R. Golestanian, Phys. Rev. E 75 (2007) 040103.
[27] F. Tajik, A.A. Masoudi, M. Sedighi, G. Palasantzas, Chaos 30 (2020) 073101.
[28] M. Antezza, L.P. Pitaevskii, S. Stringari, V.B. Svetovoy, Phys. Rev. A 77 (2008) 022901;
M. Antezza, L.P. Pitaevskii, S. Stringari, V.B. Svetovoy, Phys. Rev. Lett. 97 (2006) 223203.
[29] J.M. Obrecht, R.J. Wild, M. Antezza, L.P. Pitaevskii, S. Stringari, E.A. Cornell, Phys. Rev. Lett. 98 (2007) 063201.
[30] G.L. Klimchitskaya, V.M. Mostepanenko, R.I.P. Sedmik, Phys. Rev. A 100 (2019) 022511.
[31] G. Palasantzas, J.T.M. DeHosson, Phys. Rev. B 72 (2005) 115426.
[32] F. Tajik, Z. Babamahdi, M. Sedighi, A.A. Masoudi, G. Palasantzas, Chaos 29 (2019) 093126.
[33] F. Tajik, A.A. Masoudi, Z. Babamahdi, M. Sedighi, G. Palasantzas, Chaos 30 (2020) 023108.
[34] M. Sedighi, G. Palasantzas, J. Appl. Phys. 117 (2015) 144901.
[35] F. Tajik, M. Sedighi, A.A. Masoudi, H. Waalkens, G. Palasantzas, Phys. Rev. E 100 (2019) 012201.
[36] M. Sedighi, V.B. Svetovoy, W.H. Broer, G. Palasantzas, Phys. Rev. B 89 (2014) 195440.
[37] M. Sedighi, V.B. Svetovoy, G. Palasantzas, Phys. Rev. B 93 (2016) 085434.
[38] G.L. Ingold, G.L. Klimchitskaya, V.M. Mostepanenko, Phys. Rev. A 101 (2020) 032506.
[39] R. Garcıa, R. Perez, Surf. Sci. Rep. 47 (2002) 197.
[40] A.O. Sushkov, W.J. Kim, D.A.R. Dalvit, S.K. Lamoreaux, Nat. Phys. 7 (2011) 230.
[41] S. Cui, Y.C. Soh, J. Microelectromech. Syst. 19 (2010) 1153.
[42] M. Sedighi, W.H. Broer, G. Palasantzas, B.J. Kooi, Phys. Rev. B 88 (2013) 165423.
[43] R. Esquivel-Sirvent, L. Reyes, J. Bárcenas, New J. Phys. 8 (2006) 241.
[44] W. Broer, H. Waalkens, V.B. Svetovoy, J. Knoester, G. Palasantzas, Phys. Rev. Appl. 4 (2015) 054016.
[45] J. Guckenheimer, P. Holmes, Nonlinear Oscillations, Dynamical Systems, and Bifurcations of Vector Fields, Springer-Verlag, New York Berlin Heidelberg Tokyo, 1986.
[46] O. Degani, Y. Nemirovsky, J. Microelectromech. Syst. 11 (2002) 20.
[47] M.W. Hirsch, S. Smale, R.L. Devaney, Elsevier Academic Press, San Diego, CA, 2004.
[48] F.H. Ling, G.W. Bao, Phys. Lett. A 122 (1987) 413.
[49] G.L. Klimchitskaya, V.M. Mostepanenko, Phys. Rev. A 105 (2022) 012805;
V.B. Svetovoy, R. Esquivel, Phys. Rev. E 72 (2005) 036113;
G.L. Klimchitskaya, V.M. Mostepanenko, Eur. Phys. J. C 80 (2020) 900.